Supporting Information for

Molecular Architectures of Iron Complexes for Oxygen Reduction Catalysis - Activity Enhancement by Hydroxide Ions Coupling

Poe Ei Phyu Win,[1] Jiahui Yang,[1] Shuwang Ning,[5] Xiang Huang,[3] Gengtao Fu,[5] Qiming Sun,[1,2] Xing-Hua Xia,[4]* Jiong Wang[1,2]**

[1]Innovation Center for Chemical Science, College of Chemistry, Chemical Engineering and Materials Science, Soochow University, Suzhou 215006, China

[2]Jiangsu Key Laboratory of Advanced Negative Carbon Technologies, Soochow University, Suzhou, 215123, Jiangsu, China

[3]Department of Physics, Southern University of Science and Technology, Shenzhen 518055, China

[4]State Key Laboratory of Analytical Chemistry for Life Science, School of Chemistry and Chemical Engineering, Nanjing University, Nanjing 210023, China

[5]Jiangsu Key Laboratory of New Power Batteries, Jiangsu Collaborative Innovation Center of Biomedical Functional Materials, School of Chemistry and Materials Science, Nanjing Normal University, Nanjing 210023, China

E-mail: huangx8@sustech.edu.cn (X. H.); xhxia@nju.edu.cn (X. X.); wangjiong@suda.edu.cn (J. W.)

Experiments

Synthesis of rGO. Graphene oxide (GO) was synthesized using a modified Hummers' method. In brief, graphite powder (6 g) was mixed with potassium persulfate ($K_2S_2O_8$, 2 g) and phosphorus pentoxide (P_2O_5, 2 g) in 98 % sulfuric acid (H_2SO_4) being heated at 80 ^oC for 10 h. Afterwards the product was continued to react with potassium permanganate ($KMnO_4$, 6 g) in 98 % H_2SO_4 at 40 ^oC for 2 h, achieving GO. To obtain the reduced GO (rGO), the resultant GO was transferred into a Teflon lined stainless autoclave, and was heated at 150 ^oC for 3 h.

Synthesis of FePc NTs-rGO. Iron phthalocyanine nanotubes (FePc NTs) were synthesized by a simple hydrothermal method. A 5.76 mmol of phthalonitrile ($C_8H_4N_2$), 1.44 mmol of iron(II) acetate tetrahydrate ($C_4H_{14}FeO_8$), and 10 mg of ammonium heptamolybdate tetrahydrate ($(NH_4)_6Mo_7O_{24}{\cdot}4H_2O$) were put in ethylene glycol solvent and stirred for 30 min. The solution was poured into a 100 mL autoclave lined with Teflon, and the autoclave temperature was kept at 180 °C for 12 h. After naturally cooling to ambient temperature, the precipitate was accrued and further washed with hydrochloric acid (HCl) of 1.0 M concentration, hot water and ethanol for several times for the removal of residual reagents. The resultant FePc NTs were dried in a vacuum oven at 60 °C for 24 h. Secondly, the rGO (5 mg) was dispersed into *N, N*-dimethylformamide (DMF) containing FePc NTs (10 mg). The FePc NTs-rGO suspension was heated at 80 ^oC for 12 h. Then the suspension was centrifuged to remove free FePc NTs in DMF, and FePc NTs-rGO was washed with ethanol and dispersed in isopropanol (2 mg mL^{-1}).

Synthesis of FePc-rGO. 10 mg of FePc was dissolved in DMF, and was mixed with 5 mg of rGO (dispersed in DMF) to be heated to 80 ^oC for 12 h. The resultant mixture was centrifuged to remove any free FePc remained in DMF. Then it was washed with ethanol to achieve FePc-rGO, and dispersed in isopropanol (2 mg mL^{-1}).

Synthesis of FePc Agg-rGO. 10 mg of FePc powders and 5 mg of rGO powders were directly mixed using a mortar and pestle to thoroughly combine the two materials, and the resultant mixtures were directly dispersed in isopropanol (2 mg mL^{-1}).

Rotating ring-disk electrode (RRDE) measurements. For the RRDE measurements, a glassy carbon (GC) disk (5.6 mm in diameter) and a Pt ring (0.9 mm in width) were applied as the working electrodes fixed on a rotating apparatus (PINE Company). The ORR electrochemical measurements were performed on a CHI 1140C potentiostat (CH Instrument Company) with a Hg/HgO electrode and a graphite rod as the reference and counter electrodes, respectively. Prior to electrochemical measurements, the GC disk and Pt ring electrodes were polished with 0.05 μm alumina slurries. Then the electrodes were successively sonicated in ethanol and deionized water. Before the RRDE measurements, the Pt ring electrode was further electrochemically polished in 0.5 M H_2SO_4 with continuous cyclic voltammetry scanning between -0.65 V to 0.9 V vs $Hg/HgSO_4$ until the polarization curves became highly repeatable. A 10 μL of suspension (2 mg mL^{-1} samples dispersed in isopropanol) was cast on the GC disk and was later dropped Nafion solution (0.5 wt% in isopropanol) without contacting the Pt ring. The ink was dried slowly in air until a uniform catalyst distribution across the electrode surface was obtained. For comparison, the 20% Pt/C (the same loadings on GC disk as the cases of FePc based samples) was also electrochemically polished in 0.5 M H_2SO_4 with continuous cyclic voltammetry scanning between -0.65 V to 0.9 V vs $Hg/HgSO_4$ until the polarization curves became highly repeatable before the RRDE measurements. Then the electrolyte was changed into 0.1 M KOH purged with O_2 for conducting the ORR measurement. The selectivity of producing HO_2^-(%) and the electron transfer number (n) were determined by the following equations S-1 and S-2,

$$HO_2^-(\%) = 200 \times \frac{I_r/N}{I_d + I_r/N} \qquad \text{(S-1)}$$

$$n = 4 \times \frac{I_d}{I_d + I_r/N} \qquad \text{(S-2)}$$

where I_d is disk current, I_r is ring current and N is current collection efficiency of the Pt ring.

Zinc-air battery. To approach the practical use, we assembled the liquid zinc-air battery using FePc NTs-rGO as the cathode catalyst. The liquid zinc-air battery tests were operated in a homemade zinc-air cell. The electrocatalyst ink was prepared by mixing 10 mg of electrocatalysts and of 250 μL solution, in which 250 μL of solution was prepared by mixing 100 μL of deionized water, 100 μL of methanol, and 50 μL of Nafion. The air cathode consists of porous carbon paper with a gas diffusion layer (GDL) loaded with FePc NTs-rGO or commercial Pt/C catalyst. The anode consisted of a 0.3 mm zinc plate. The electrolyte for the zinc-air battery was 0.2 M $ZnCl_2$

contained in 6 M KOH solution. The battery test for open-circuit voltage (OCV) and power density was performed on a CHI 760E potentiostat.

***In situ* electrochemical Raman measurements.** The measurements were conducted on a commercial three-electrode electrochemical cell with one quartz window filling 0.1 M KOH with continuously purging O_2. An Ag/AgCl wire (soaked in saturated KCl solution) and carbon rod were used as the reference electrode and counter electrode, respectively. A glassy carbon plate coated with the catalyst was used as the working electrode. The acquisition time was set to 60 s with 638 nm laser (25% of power density). Each spectral data was accumulated twice.

Calculation of TOFs.

$$TOF = i_k / (4 \times F \times m) \qquad \text{(S-3)}$$

where i_k is the kinetic ORR current derived from the Koutecky-Levich analysis; F is the Faraday constant; m is the Fe content on the electrode surface, which was determined by the ICP measurement.

Laviron equation.

$$E_c = E_{1/2} - (\frac{RT}{\alpha nF}) \times \mathrm{In}\,(\frac{\alpha nF}{RTk_s}) - (\frac{RT}{\alpha nF}) \times \mathrm{In}\,(v) \qquad \text{(S-4)}$$

where E_c is the reduction potential of metal redox, $E_{1/2}$ is the formal potential of metal redox, R is the universal gas constant, T is the temperature in kelvin, n is the number of electrons transferred, α is the transfer coefficient, k_s is the kinetic constant of metal redox, and v is the scan rate in the CV measurement.

Computational method. Spin-polarized density functional theory calculations were performed at the generalized gradient approximation with the grid-based projector augmented wave (GPAW)[1] code and atomic simulation environment (ASE)[2]. The electronic wavefunctions were represented on a uniform real-spaced grid with a spacing of 0.2 Å, and the Fermi smearing width was set to 0.1 eV. The exchange-correlation and van der Waals contributions are considered using the BEEF-vdW functional.[3] For the structure optimization, we utilized an orthorhombic cell with vacuum layers of ~15 Å. The Brillouin zone is sampled at the Gamma point. All the atoms were relaxed

until the force on each atom was less than 0.05 eV/Å. The reaction energy of an electrochemical step containing coupled proton and electron pair was calculated using the computational hydrogen electrode (CHE) model.[4] The entropy and zero-point energy corrections are used to evaluate the Gibbs free energy.[5] In addition, to account for the solvation effect, *OH and *OOH are stabilized by -0.15 eV due to the hydrogen bonding with water.[6]

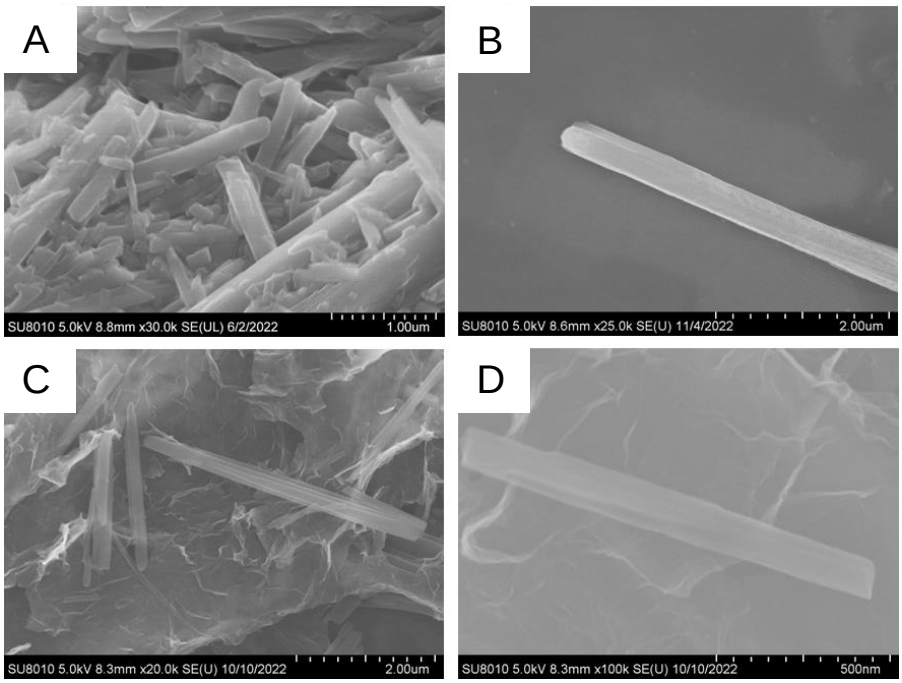

Fig. S1. SEM images of FePc NTs (A, B) and FePc NTs-rGO (C, D) at different resolutions.

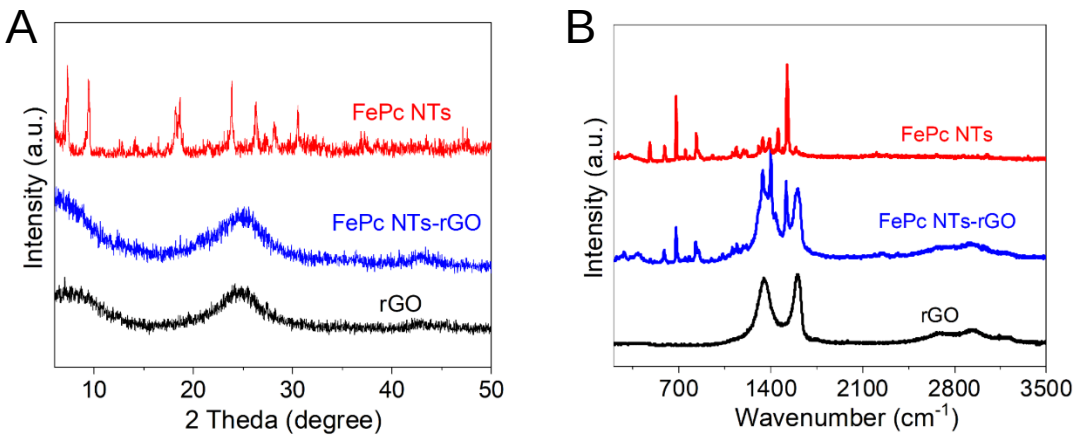

Fig. S2. XRD patterns (A) and Raman spectra (B) of rGO, FePc NTs and FePc NTs-rGO.

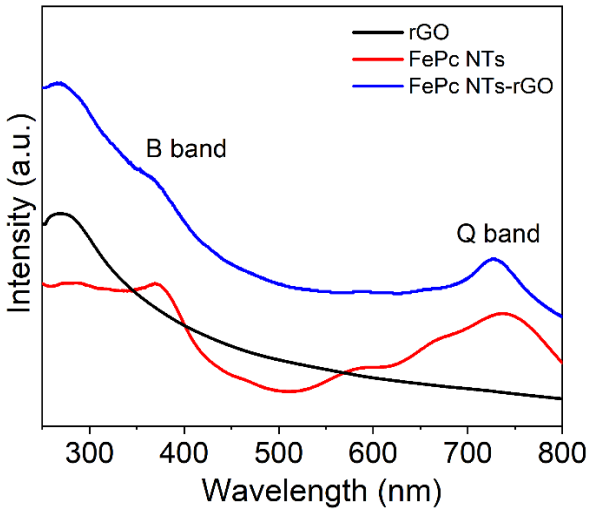

Fig. S3. UV-vis spectra of FePc NTs and FePc NTs-rGO. The pristine rGO is included as background. The UV-vis data were collected in DMF.

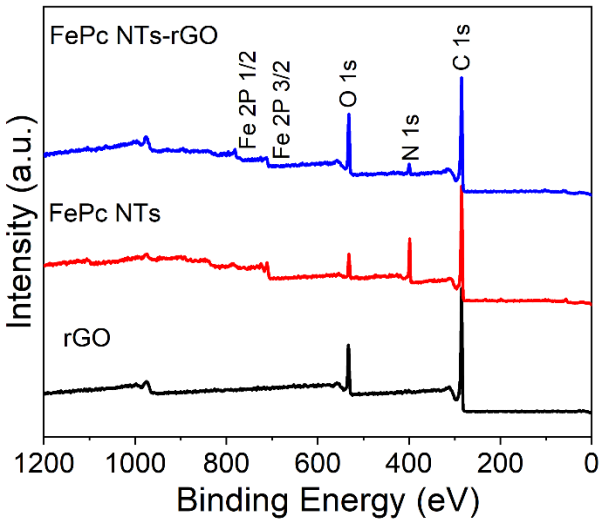

Fig. S4. XPS full elemental surveys of rGO, FePc NTs and FePc NTs-rGO.

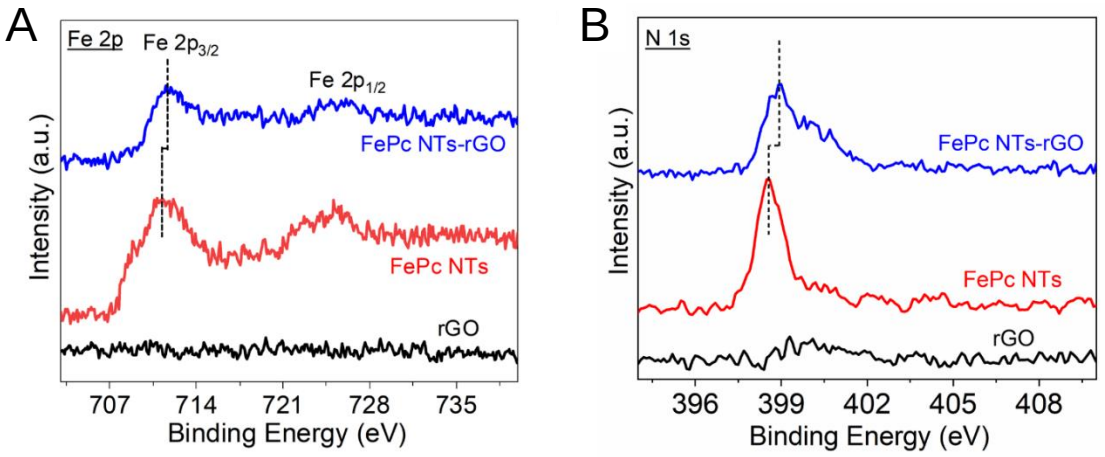

Fig. S5. XPS surveys of Fe 2*p* (A) and N 1*s* (B) core electron levels of FePc NTs and FePc NTs-rGO. The pristine rGO is included as background.

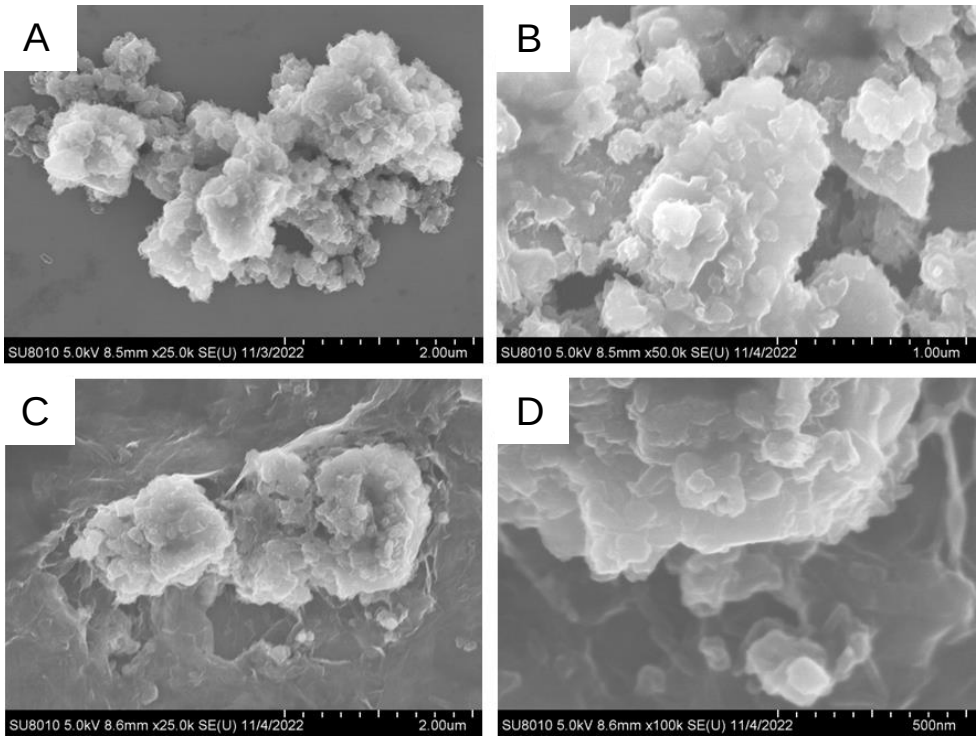

Fig. S6. SEM images of FePc Agg (A, B) and FePc Agg-rGO (C, D) at different resolutions.

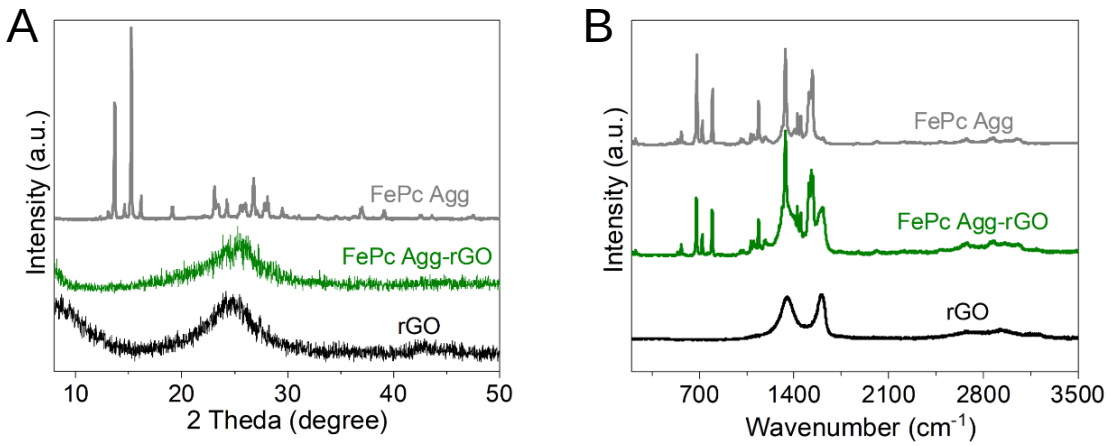

Fig. S7. XRD patterns (A) and Raman spectra (B) of rGO, FePc Agg and FePc Agg-rGO.

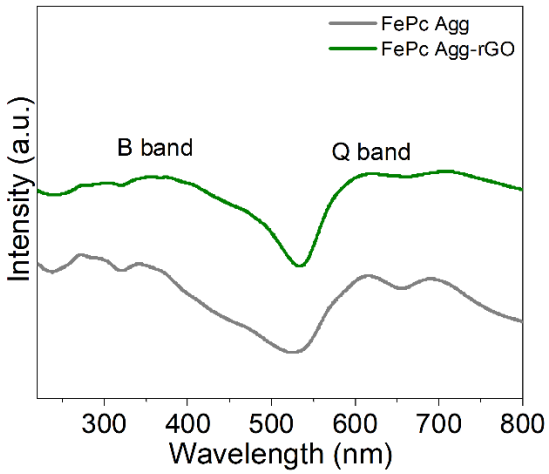

Fig. S8. UV-vis spectra of FePc Agg and FePc Agg-rGO conducted in isopropanol.

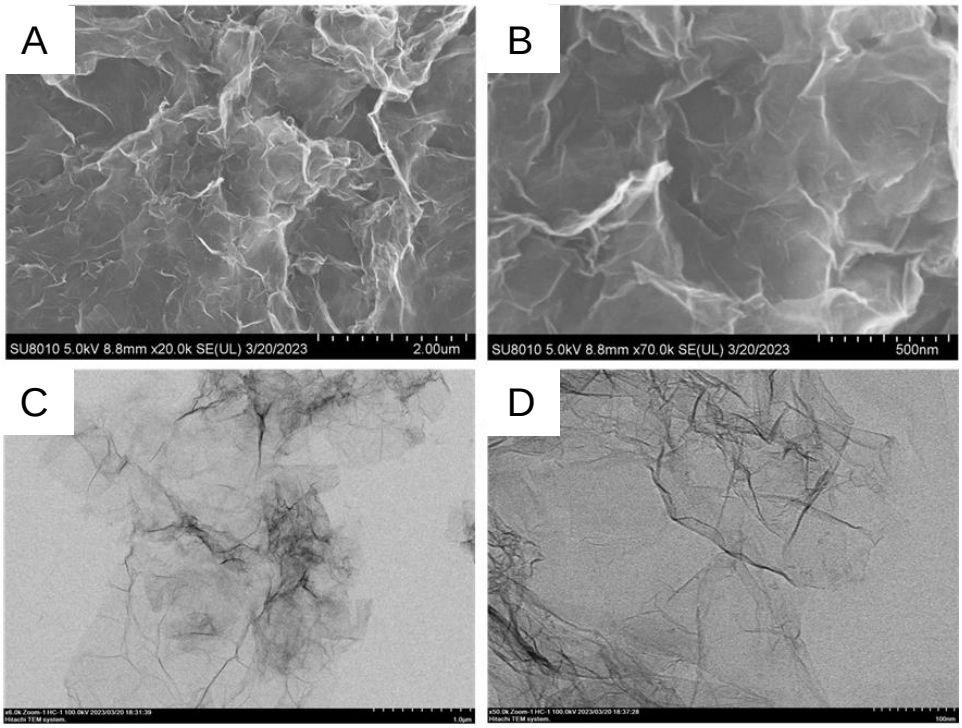

Fig. S9. SEM (A, B) and TEM (C, D) images of FePc-rGO at different resolutions.

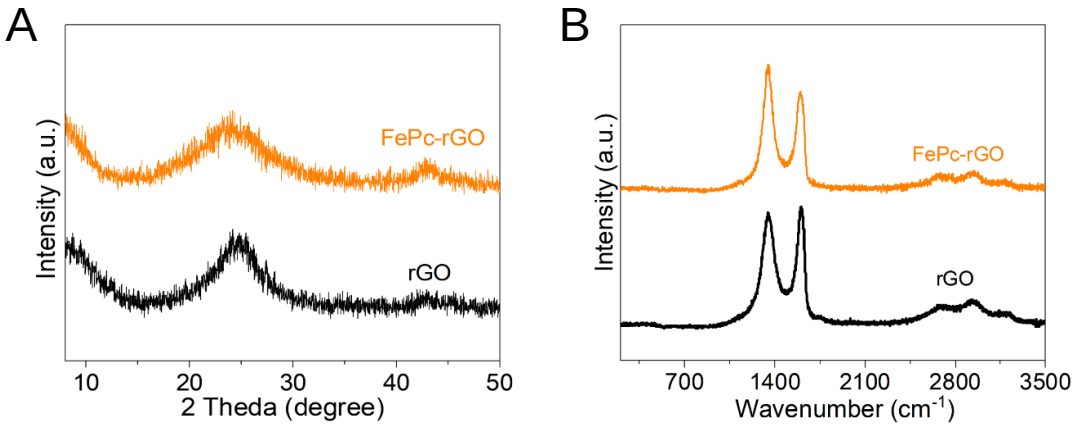

Fig. S10. XRD patterns (A) and Raman spectra (B) of rGO and FePc-rGO.

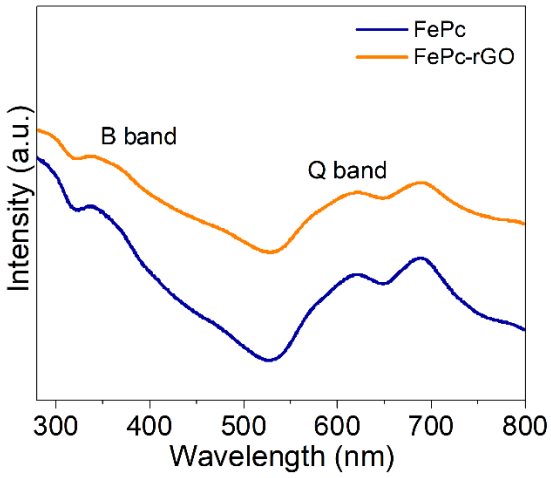

Fig. S11. UV-vis spectra of FePc and FePc-rGO in DMF.

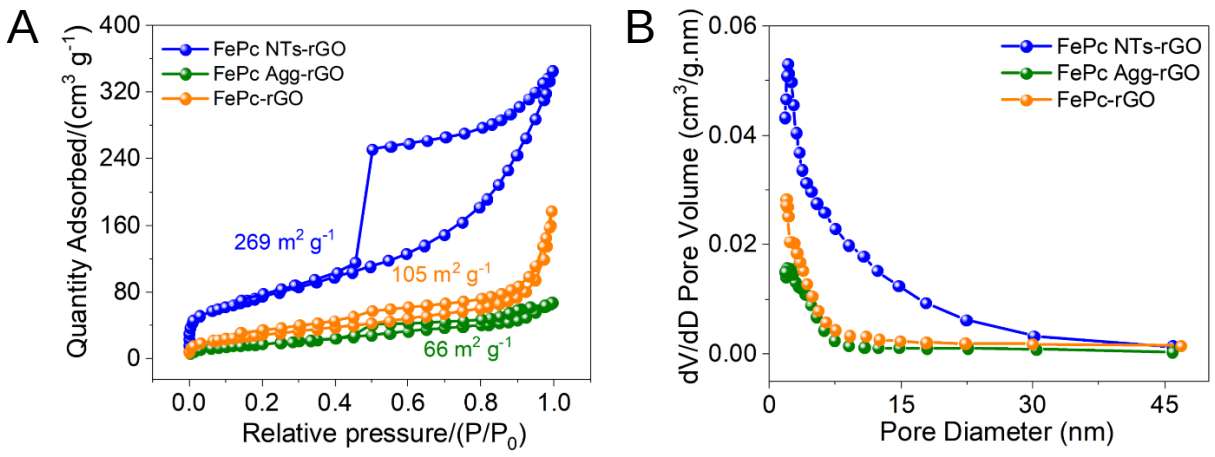

Fig. S12. (A) N_2 adsorption/desorption isotherms of FePc NTs-rGO, FePc Agg-rGO and FePc-rGO collected at 77 K and (B) corresponding pore size distribution.

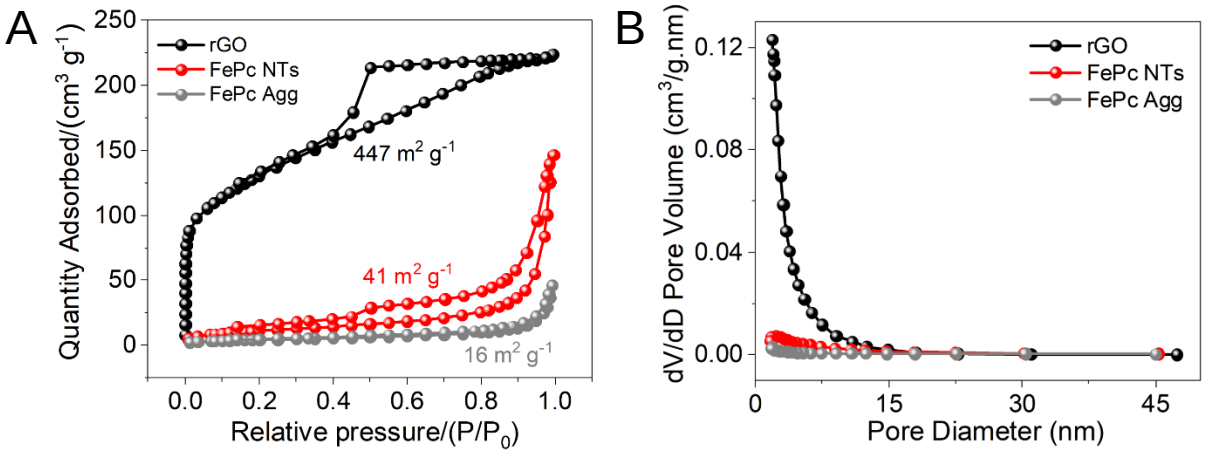

Fig. S13. (A) N_2 adsorption/desorption isotherms of rGO, FePc NTs and FePc Agg collected at 77 K and (B) corresponding pore size distribution.

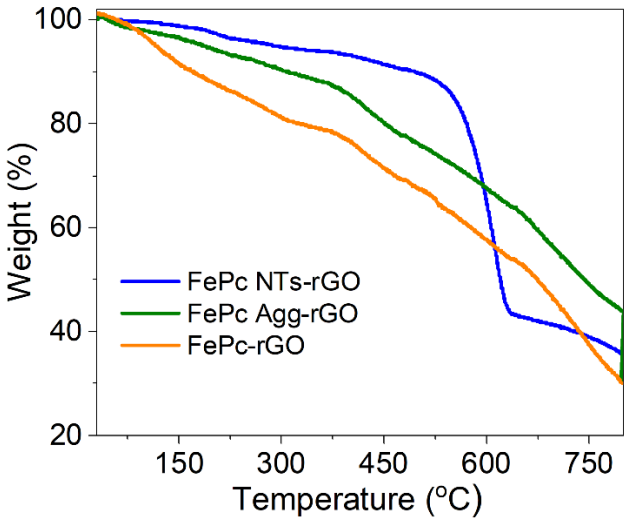

Fig. S14. Thermogravimetric analysis of FePc NTs-rGO, FePc Agg-rGO and FePc-rGO under N_2 atmosphere.

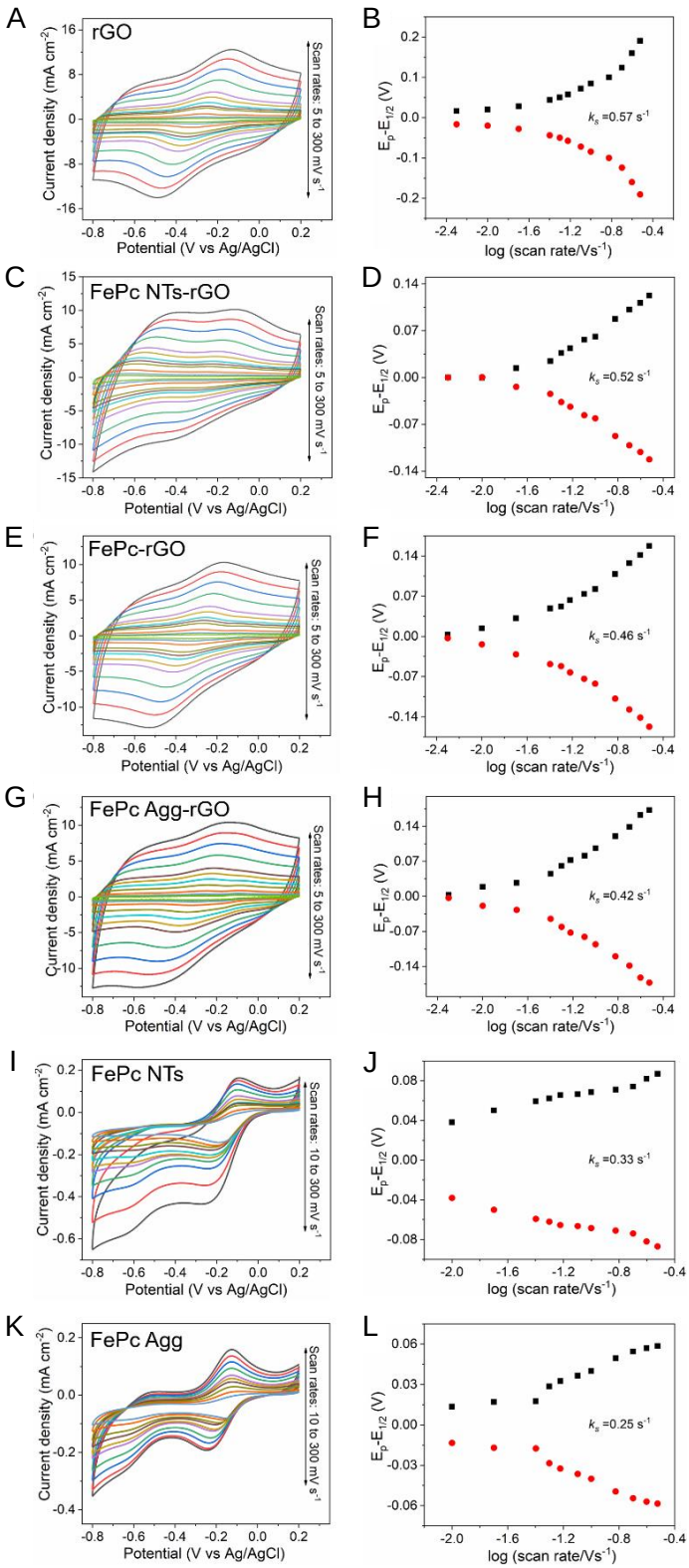

Fig. S15. CVs (left column) of various samples conducted in 1 mM $Ru(NH_3)_6Cl_3$/0.1 M KCl with various scan rates, and the corresponding Laviron analytical results (right column).

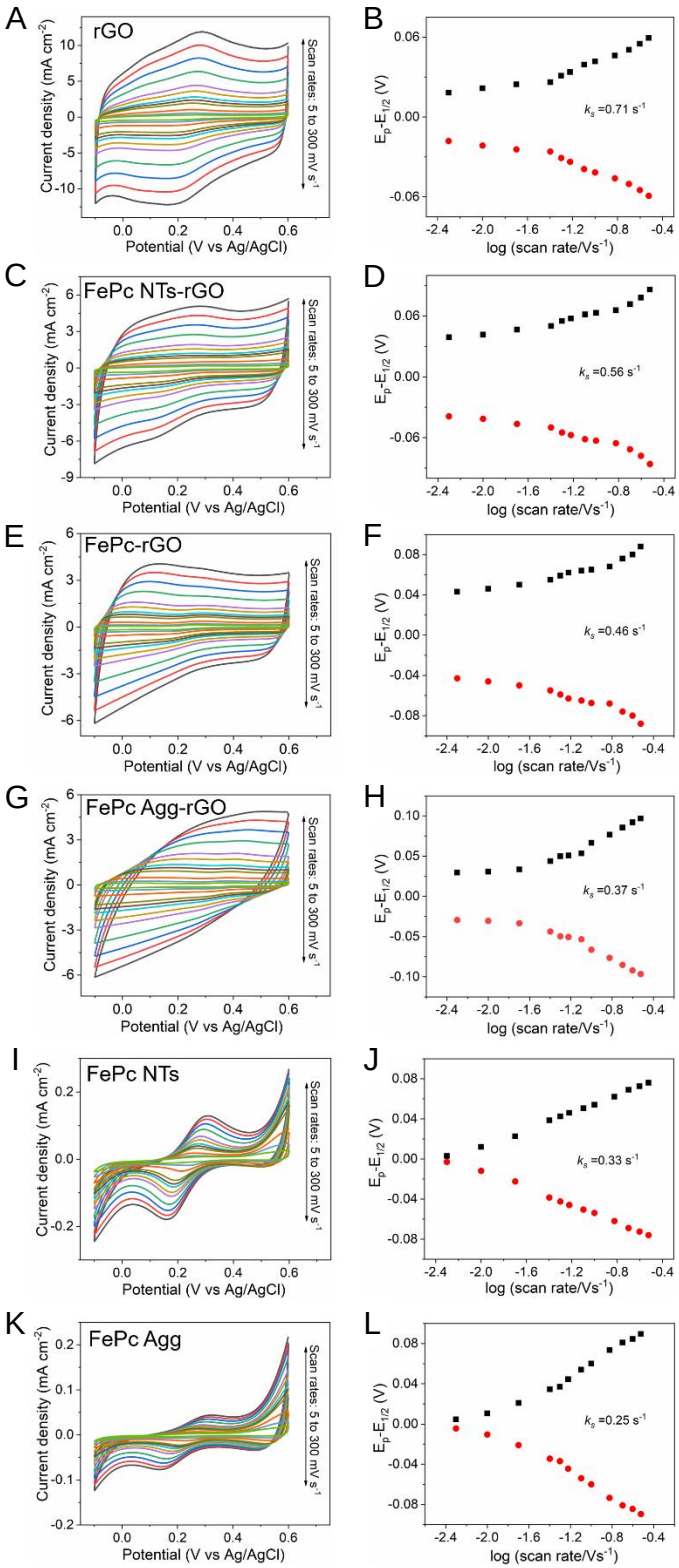

Fig. S16. CVs (left column) of various samples conducted in 1 mM $K_3Fe(CN)_6$/0.1 M KCl with various scan rates, and the corresponding Laviron analytical results (right column).

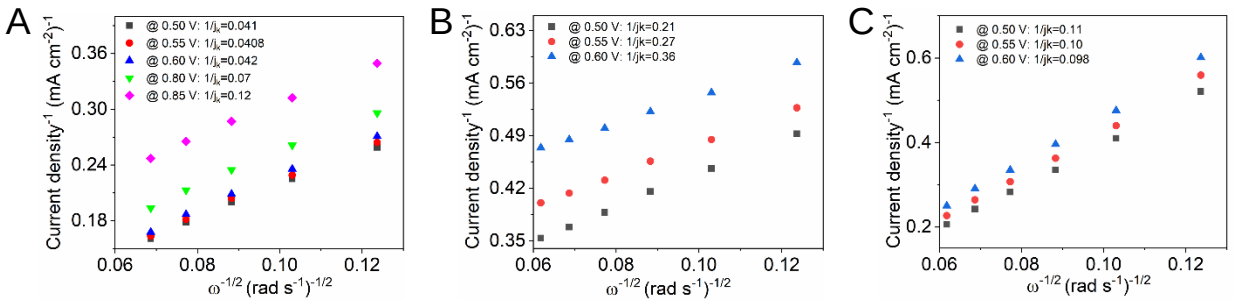

Fig. S17. Koutecky-Levich plots of FePc NTs-rGO (A), FePc Agg-rGO (B) and FePc-rGO (C). The data were recorded in O_2 saturated 0.1 M KOH.

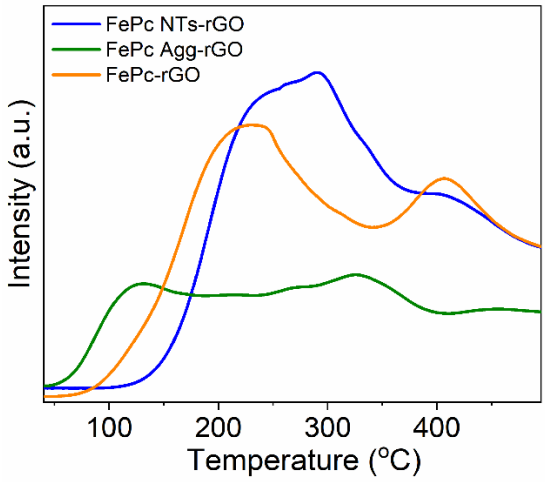

Fig. S18. Temperature programmed desorption curves of O_2 for various samples.

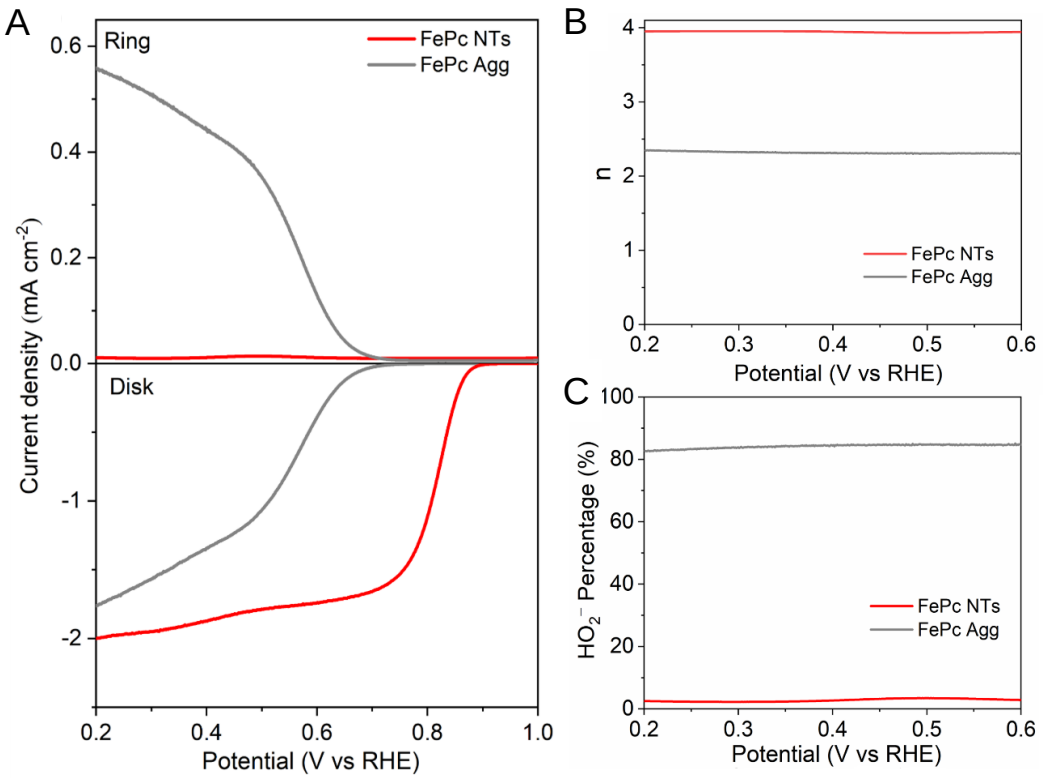

Fig. S19. (A) RRDE measurements recorded with FePc NTs and FePc Agg in O_2 saturated 0.1 M KOH, 1600 rpm, 10 mV s^{-1}. Corresponding n values (B) and HO_2^- percentage (C) of ORR derived from the RRDE data.

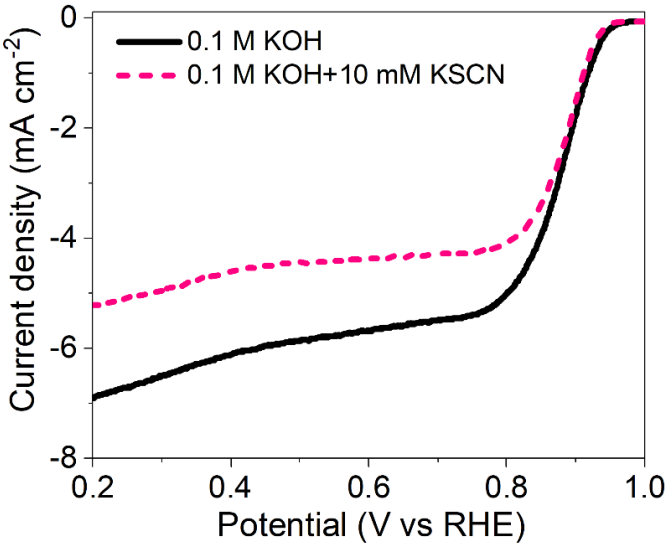

Fig. S20. LSVs of FePc NTs-rGO in O_2 saturated 0.1 M KOH with and without adding 10 mM of KSCN at a rotation speed of 1600 rpm.

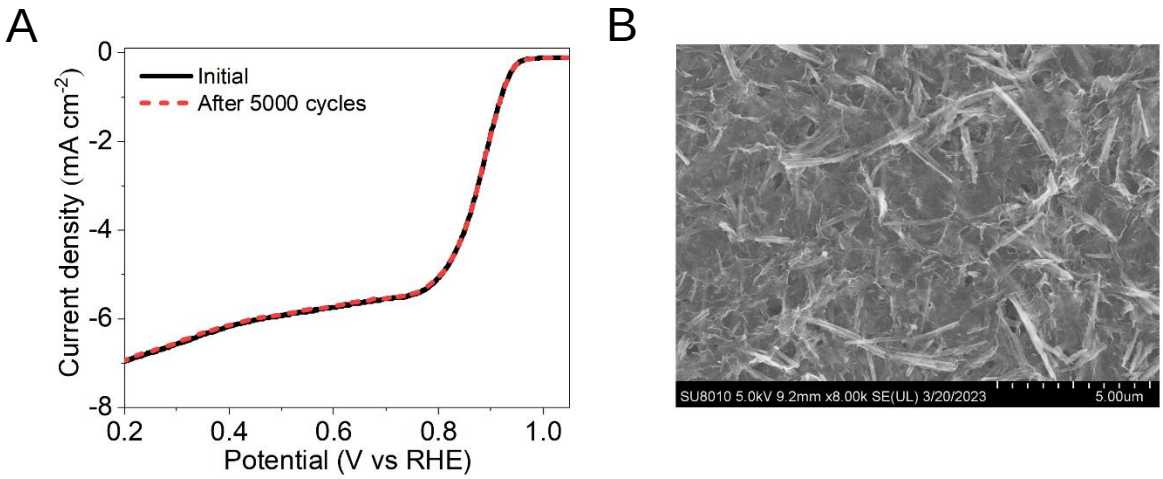

Fig. S21. (A) LSVs of FePc NTs-rGO before and after 5000 cycles in O_2 saturated 0.1 M KOH at a rotation rate of 1600 rpm. (B) A typical SEM image of FePc NTs-rGO after 5000 ORR cycles.

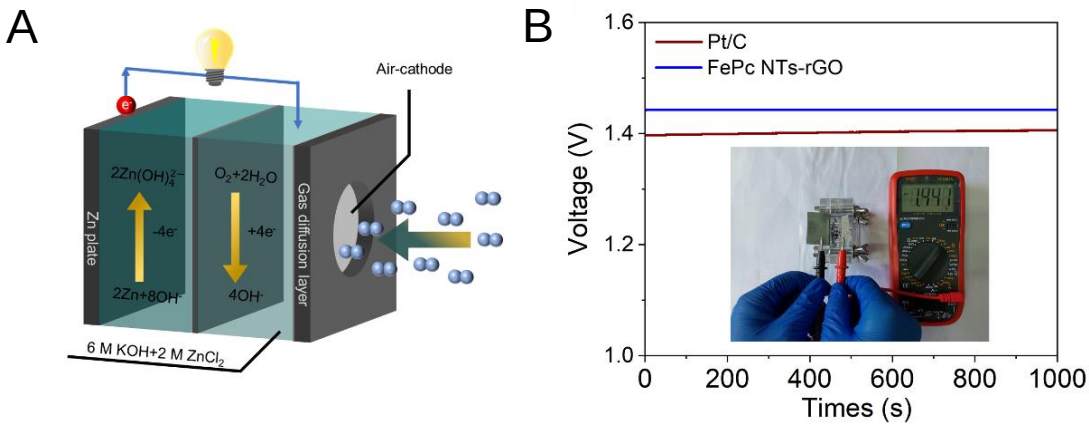

Fig. S22. (A) Scheme illustrates a zinc-air battery. (B) OCV of the assembled battery using FePc NTs-rGO as the cathode catalyst compared with the battery using Pt/C catalyst.

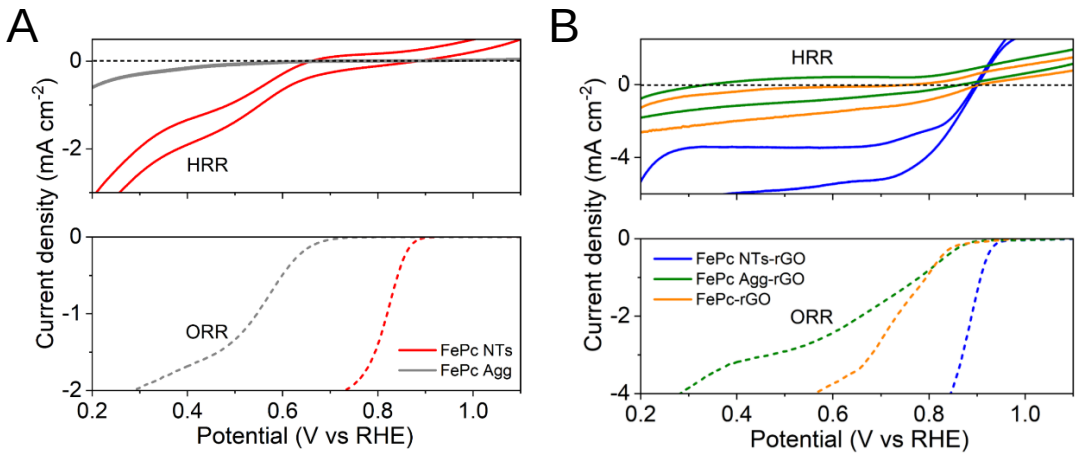

Fig. S23. (A) Redox of H_2O_2 on the pristine FePc NTs and FePc Agg, 50 mV s^{-1}, 40 μM H_2O_2, 0.1 M KOH, N_2 atmosphere, 1600 rpm. (B) Redox of H_2O_2 on FePc NTs-rGO, FePc Agg-rGO and FePc-rGO collected at the same condition. The corresponding ORR polarization curves are also included for comparison.

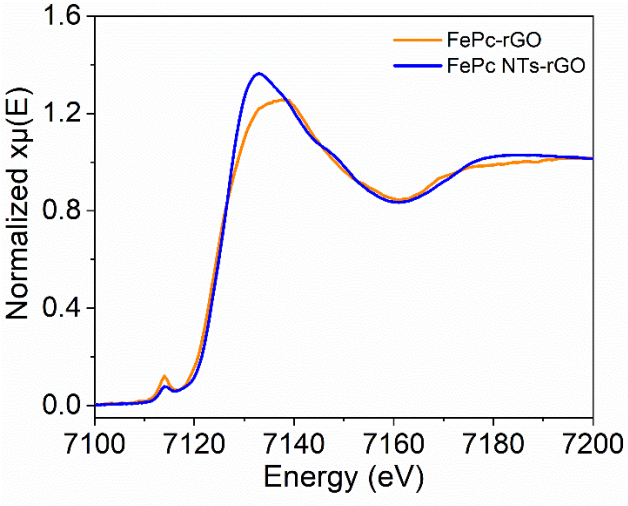

Fig. S24. Fe K-edge XANES data of FePc-rGO and FePc NTs-rGO.

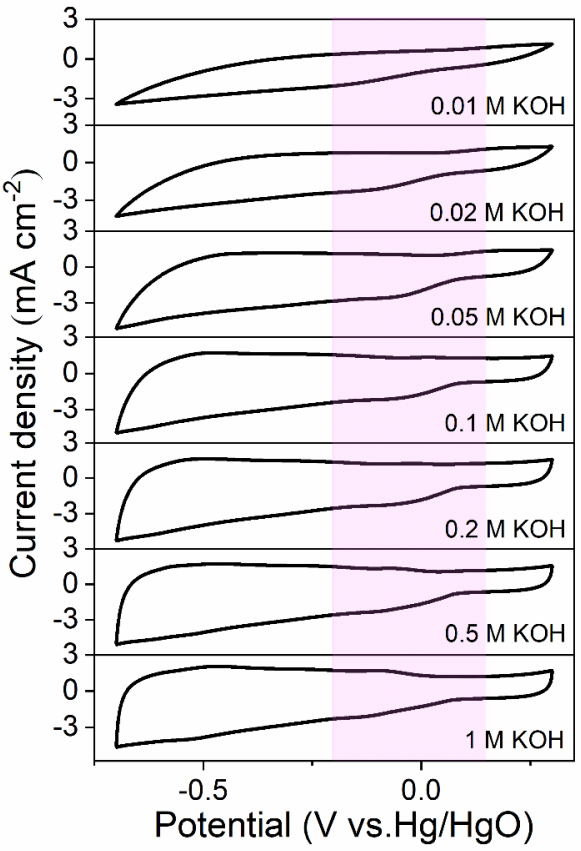

Fig. S25. CVs of FePc-rGO in KOH solutions with different pH values at a scan rate of 50 mV s^{-1}.

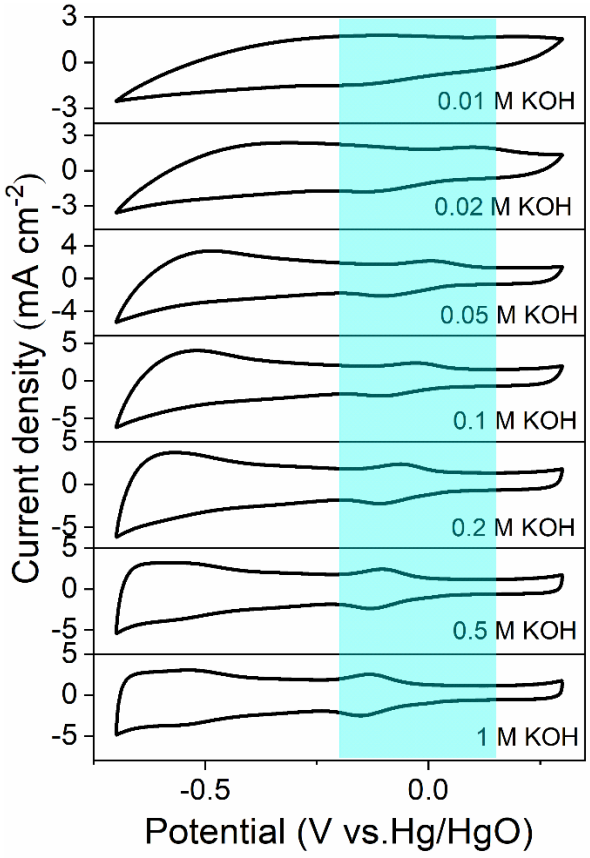

Fig. S26. CVs of FePc NTs-rGO in KOH solutions with different pH values at a scan rate of 50 mV s^{-1}.

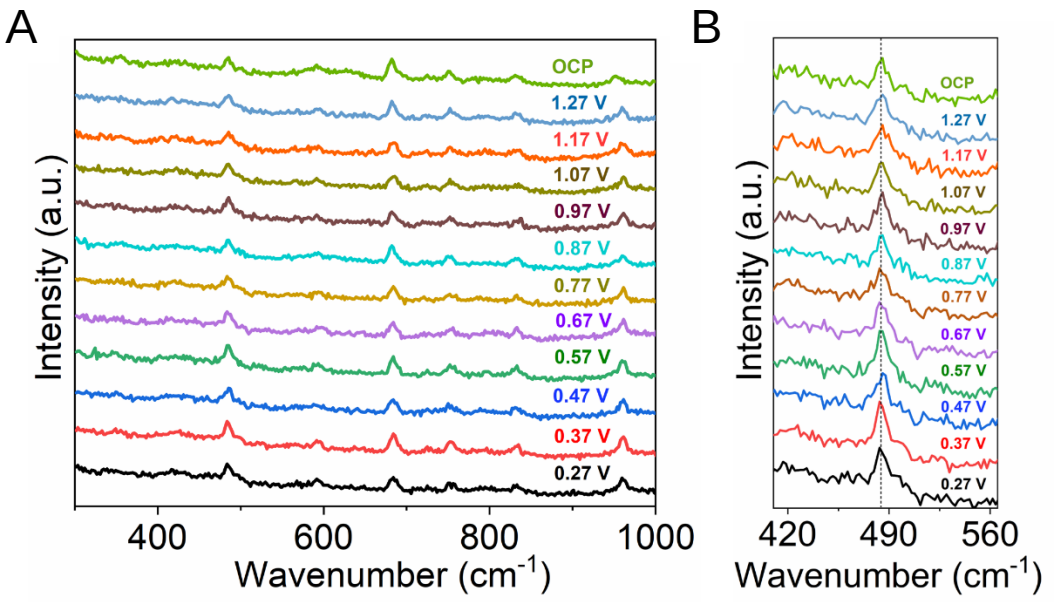

Fig. S27. (A) *In situ* Raman electrochemical measurements of FePc NTs-rGO conducted in 0.1 M KOH under O_2 atmosphere. The potentials applied on FePc NTs-rGO ranged from 1.27 V to 0.27 V. (B) The Raman spectra amplified around 591 cm^{-1} at the various potentials.

Table S1. Fe contents of FePc NTs-rGO, FePc Agg-rGO and FePc-rGO as measured by inductively coupled plasma spectroscopy.

Samples	Fe Contents (mol mg^{-1})
FePc NTs-rGO	1.2×10^{-6}
FePc Agg-rGO	1.4×10^{-6}
FePc-rGO	0.96×10^{-6}

Table S2. Fe contents achieved from the surfaces of FePc NTs-rGO, FePc Agg-rGO and FePc-rGO modified electrodes as measured by inductively coupled plasma spectroscopy.

Samples	Fe contents on electrode surfaces (mol cm^{-2})	Standard deviation (mol cm^{-2})
FePc NTs-rGO	8.9×10^{-8}	1.5×10^{-8}
FePc Agg-rGO	8.2×10^{-8}	4.1×10^{-9}
FePc-rGO	7.1×10^{-8}	8.4×10^{-9}

In the above measurements, FePc NTs-rGO, FePc-rGO and FePc Agg-rGO modified carbon electrodes (5 mm in diameter) were directly immersed into concentrated nitric acid for 10 min and diluted by addition of Millipore water for the ICP measurements.[7] The electrodes remained in the Teflon holders during the acid digestion to ensure that only the electrochemically relevant surface was analyzed. The contribution of Fe impurities from acid were excluded.

References

(1) Mortensen, J. J.; Hansen, L. B.; Jacobsen, K. W. Real-space grid implementation of the projector augmented wave method. *Phys. Rev. B* **2005**, *71*, 035109.

(2) Bahn, S. R.; Jacobsen, K. W. An object-oriented scripting interface to a legacy electronic structure code. *Comput. Sci. Eng.* **2002**, *4*, 56-66.

(3) Wellendorff, J.; Lundgaard, K. T.; Møgelhøj, A.; Petzold, V.; Landis, D. D.; Nørskov, J. K.; Bligaard, T.; Jacobsen, K. W. Density functionals for surface science: Exchange-correlation model development with Bayesian error estimation. *Phys. Rev. B* **2012**, *85*, 235149.

(4) Nørskov, J. K.; Rossmeisl, J.; Logadottir, A.; Lindqvist, L.; Kitchin, J. R.; Bligaard, T.; Jónsson, H. Origin of the Overpotential for Oxygen Reduction at a Fuel-Cell Cathode. *J. Phys. Chem. B* **2004**, *108*, 17886-17892.

(5) Wan, H.; Østergaard, T. M.; Arnarson, L.; Rossmeisl, J. Climbing the 3D Volcano for the Oxygen Reduction Reaction Using Porphyrin Motifs. *ACS Sustainable Chem. Eng.* **2019**, *7*, 611-617.

(6) Back, S.; Kulkarni, A. R.; Siahrostami, S. Single Metal Atoms Anchored in Two-Dimensional Materials: Bifunctional Catalysts for Fuel Cell Applications. *ChemCatChem* **2018**, *10*, 3034-3039.

(7) Oh, S.; Gallagher, J. R.; Miller, J. T.; Surendranath, Y. Graphite-Conjugated Rhenium Catalysts for Carbon Dioxide Reduction. *J. Am. Chem. Soc.* **2016**, *138*, 1820-1823.